Physics Letters A 483 (2023) 129040

Contents lists available at ScienceDirect

Physics Letters A

journal homepage: www.elsevier.com/locate/pla

Mechanical, electronic and thermodynamic properties of crystalline molecular hydrogen at high pressure

Xiao-Yong Yang [a], Rajeev Ahuja [a,b], Wei Luo [a,*]

[a] Materials Theory, Department of Physics and Astronomy, Uppsala University, Box 516, 75120 Uppsala, Sweden
[b] Department of Physics, Indian Institute of Technology Ropar, Rupnagar 140001, Punjab, India

ARTICLE INFO

Article history:
Received 1 June 2023
Received in revised form 18 July 2023
Accepted 21 July 2023
Available online 7 August 2023
Communicated by J.G. Lu

Keywords:
High-pressure hydrogen
First-principle calculations
Mechanical property
Electronic property
Phonon dispersion curves

ABSTRACT

Solid molecular hydrogen exhibits a rich variety of unique properties, including insulator-to-metal transition. However, the specific structure of phase III remains unclear. Experimental evidence suggests high-pressure hydrogen shows a hexagonal close-packed lattice. Therefore, as a potential candidate for phase III, the structure, energetic, mechanical, electronic, and thermodynamic properties of $P6_122$ structure are systemically studied. It is found phase III with $P6_122$ space group is both mechanically and thermodynamically stable within the pressure range of 120∼300 GPa. Besides, we observed significant enhancements in the bulk modulus, shear modulus, and Young's modulus. The band structures exhibit a transition from topological insulator to topological semiconductor and eventually to a Wely semimetal as the pressure increases. The electron density accumulates between pseudo "H_2" molecules in the insulating phase but it partly channels into the interlayer space in the semimetallic phase. Phase III with $P6_122$ structure is barely explored previously in solid hydrogen, therefore, we believe our present investigation contributes valuable insights towards understanding the behavior of metallic hydrogen.

1. Introduction

Solid molecular hydrogen under high pressure has garnered significant interest in the field of condensed matter physics for more than a century [1]. However, the experimental determination of precise structures for solid hydrogen and deuterium has been a significant challenge, mainly due to the limitations of low-resolution diffraction models when subjected to *x*-ray radiation. To date, seven high-pressure solid phases of hydrogen have been reported. Phase I (near 800 cm^{-1} [2]) is energetically stable in the pressure range of 5 GPa to 190 GPa at room temperature. In this phase, hydrogen molecules exhibit rotational disorder with a hexagonal close-packed (hcp) solid structure, as determined through single-crystal *x*-ray diffraction (SXRD) [3,4]. Phase II is a low-temperature phase that remains stable between 70 GPa and 160 GPa at temperatures below 135 K and exhibits minor shifts in Raman and IR spectra, near 900-1000 cm^{-1} [5,6]. This phase reveals the quantum orientational ordering of hydrogen molecules on hcp sites. For deuterium, a similar phase known as phase II′ exists within the pressure range of 20 GPa to 100 GPa below 130 K [7]. Phase III emerges above 150 GPa at low temperatures and exhibits significant shifts, splitting, and intensification in Raman and infrared vibrations and rotations, which is interpreted as the classical orientational ordering of solid hydrogen molecules [1]. Specifically, the full width at half maximum (FWHM) of the vibrational mode ν_1 reaches ∼460 cm^{-1} at ∼190 GPa, reflecting changes at the transition [8]. These observations of the low energy broad band are similar to the band at 460 cm^{-1} in H_2-III at 178 GPa and 18 K [6]. As pressure is increased above 220 GPa and the ν_1 mode reaches a frequency of ∼3800 cm^{-1}, a new transition to phase IV starts. Correspondingly, a new vibrational mode of ν_2 appears with ∼4150 cm^{-1} at 235 GPa [8]. Furthermore, based on acoustic phonon spectra from the neutron diffraction experiment, it has been confirmed that hydrogen molecules remain centered on hcp lattice sites [9]. Phase IV crystallizes in a mixed atomic-molecular state above 220 GPa at room temperature. It displays two vibrational modes with pressure-dependent broadening and a discontinuous drop in the Raman active vibration mode, which are ν_1 with ∼2750 cm^{-1} and ν_2 with ∼4150 cm^{-1} [8]. This phase is predicted to have alternating molecular and graphene-like layers based on fundamental structural changes [10]. Two additional phases, IV′ [11] and V [12], have been proposed at room temperature, corresponding to pressures of 270 GPa and 325 GPa, respectively. Their structures are slightly modified based on phase IV [13]. Importantly, hydrogen undergoes a transition to a metallic state at room temperature under pressures of 260-270 GPa [14].

* Corresponding author.
E-mail address: wei.luo@physics.uu.se (W. Luo).

https://doi.org/10.1016/j.physleta.2023.129040

The transition pressure for solid hydrogen to become a metal can be further increased to 350-360 GPa at 200 K [15], 425 GPa at 80 K [16], and 495 GPa at 5.5 K [17]. Among these phases, only phase I has been confirmed to possess an hcp structure [3,4]. Phase III exhibits spectral changes that have led to uncertainties regarding its metallic nature [18]. In addition, the molecular orientation in phase III has not been definitively confirmed [8]. More recently, experimental evidence has confirmed that phase IV is isostructural to phase III [9], and the phase transition occurs at the lowest temperature of 5 K under pressures above 360 GPa [19]. Unfortunately, experimental information for phase IV′ and V is not accessible yet. But these results have inspired many theoretical studies aimed at determining the electronic and structural properties of hydrogen at high pressure with different orientations to accurately interpret experimental observations.

While experimental methods, such as infrared (IR) and Raman vibrational spectroscopies provide an applicable way to discern the coexistence of several phases hydrogen at high pressure, i.e., bonding and structures of hydrogen as well as phase boundaries, the measurement of the crystal structure of solid hydrogen remains challenging due to the instability of diamond materials under mechanical and chemical strain, as well as the limitations of characterization techniques when operating under extreme conditions, such as *x*-ray and neutron diffraction measurements [4,8]. Recent experimental advancements have provided insights into the crystallographic nature of the transitions occurring from phase I to phases III and IV [4,17,9]. It has been discovered that under high pressure, hydrogen molecules maintain the hcp crystal structure, with a monotonic increase in anisotropy [9]. Furthermore, it has been found that the volume of the unit cell in solid hydrogen decreases linearly as pressure increases upon entering phase IV, indicating a second-order isostructural phase transition [9].

So far, extensive investigations have been conducted on the high-pressure structures of solid hydrogen using various theoretical methods, including first-principles density functional theory (DFT) methods [20,10], quantum Monte Carlo methods [21], many-body methods [21], *ab initio* molecular dynamics [22,23], and path-integral molecular dynamics [24]. In addition, using density functional perturbation theory (DFPT) based on lattice dynamics (LD), the Raman and IR frequencies as well as intensities of these structures have been simulated [25,10]. The orientation of hydrogen molecules has been identified as the key factor to determine the material's metallic or insulating behavior [4]. Several candidate structures have been proposed for high-pressure phases, including "phase II" (such as "$Pca2_1$" [26], "$P2_1/c$" [20], "$P6_3/m$" [25], and "$P63_3/mmc$" [25]) below 150 GPa and "phase III" (such as widely studied "Cmca-12" and "C2/c-24" [27]) above 150 GPa, have been investigated through static [28] and dynamic [4] density functional calculations and QMC investigations [29]. Molecular dynamics simulations based on room-temperature *x*-ray diffraction patterns (XRD) have shown similarities between hydrogen phases I, III, IV, and V [30]. Besides, the liquid-liquid transition of high-pressure hydrogen and the three hydrogen solid phases, namely the free-rotor phase I, broken-symmetry phase II, and high-pressure phase III have been respectively studied using machine-learned quantum Monte Carlo and machine-learned molecular dynamics approach [31]. The behavior of rotors on 2D-triangular, fcc and hcp lattices, interacting through the electric quadrupole-quadrupole interaction (ε_{qq}) was investigated using Markov chain Monte Carlo simulations. These simulations have demonstrated that the quadrupole-quadrupole interaction alone can stabilize various hcp-based structures [32]. Despite these successes, there is a wide range of predicted pressures for molecular dissociation and metalization, ranging from 3∼6 Mbar and 1∼3 Mbar, respectively [26]. This discrepancy is, in part, due to a lack of information about the structures and molecular orientations at megabar pressure and in part to quantum effects [13,29].

Although the electronic and structural properties of hydrogen at Mbar pressures and low temperatures are still not conclusively understood, experimental evidence has been suggested the presence of a hcp lattice above ∼150 GPa, with several possible hcp phases [9,26]. Recent theoretical findings using the *ab initio* random structure searching (AIRSS) method propose that phase III with $P6_122$ space group is the most stable phase within the pressure range of interest, exhibiting better agreement with experimental Raman and IR spectra for phase III [33]. Moreover, the hexagonal symmetry of this phase provides the best agreement with available *x*-ray diffraction data [33]. Therefore, in this study, we present a comprehensive investigation of the energetics and electronic properties, and structural stability of solid hydrogen in phase III with $P6_122$ space group, using density functional calculations within the generalized gradient approximation (GGA). In Section 2, we briefly introduce the computational method. Subsequently, in section 3, the results of GGA calculations for phase III with $P6_122$ space group at a larger number of pressures are presented and discussed. Finally, we provide a summary of this study in section 4.

2. Computational methods

Our density functional theory (DFT) calculations are carried out using the Vienna Ab initio Simulation Package (VASP) [34] with the projector-augmented-wave (PAW) potentials [34]. The exchange and correlation interactions are described by generalized gradient approximation (GGA) in the Perdew-Burke-Ernzerhof (PBE) form [35]. The valence electrons are described by a plane wave basis set with a energy cutoff of 700 eV. Integrations over the Brillouin Zone of the hexagonal cell containing 36 hydrogen atoms are done on a $17\times17\times11$ *k* grid mesh with Monkhorst-Pack scheme, which is sufficient for an energy convergence of less than 1.0×10^{-9} eV per atom. Besides, the Grimme's dispersion correction (DFT-D3) is adopted to describe the van der Waal (vdW) interactions between layered hydrogen. The spin-orbit coupling (SOC) effect is not considered in the present work for hydrogen since it is amplified for larger atoms due to the combination between the orbital angular momentum and the corresponding individual spin angular momentum [36]. The phonon spectrum is significantly connection with the dynamical stability, phase transition, thermoelectric effect, and superconductivity of the material. Thus, in the present work, we compute the phonon spectrum for solid hydrogen in phase III with $P6_122$ space group. Phonon frequency calculations are performed by using the PHONOPY package [37]. The hessian matrix is obtained by using the density functional perturbation theory (DFPT). A $2\times2\times1$ supercell containing 144 hydrogen atoms is used for DFPT calculations. The corresponding *k*-point mesh is set to be $5\times5\times7$, and the energy convergence criteria is set to be 1.0×10^{-9} eV.

3. Results and discussion

3.1. Structural property of solid hydrogen in phase III with $P6_122$ space group

Hexagonal structure of phase III with $P6_122$ space group of solid hydrogen is characterized by a primitive unit cell containing 36 atoms, with a space group (SG) No. 178, as predicted by the *ab* initio random structure searching (AIRSS) method using the Becke-Lee-Yang-Parr (BLYP) XC functional with a highly composite hydrogen number [38,33]. The layered molecular structure of the hexagonal primitive cell is depicted in Fig. 1. The optimized lattice structural details and atomic positions at 200 GPa are collected in Tables 1 and 2, respectively. For comparison, the previous results

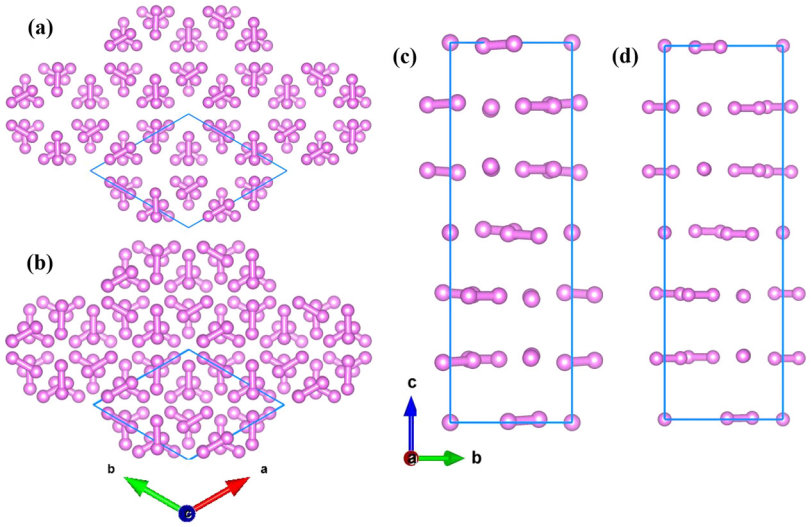

Fig. 1. (a, b) Top and (c, d) side views of layered $P6_122$ molecular structure in phase III under 50 GPa and 200 GPa, respectively.

Table 1
Lattice structural parameters, volume per proton and bond lengths between (BL) hydrogens of solid hydrogen in phase III with $P6_122$ space group at 200 GPa. For comparison, the previous results are listed here.

Phase	a (Å)	b (Å)	c (Å)	α (°)	β (°)	γ (°)	Volume per proton (Å^3)	BL1 (Å)	BL2 (Å)
$P6_122$	3.018	3.018	8.137	90.0	90.0	120.0	1.763	0.713	0.718
$P6_122$ [33]	3.022	3.022	8.143	90.0	90.0	120.0	1.789	0.719	0.715
$C2/c$-24 [33]	3.025	3.025	5.408	90.1	90.1	119.9	1.787	0.719	0.716

Table 2
Wyckoff positions, fractional atomic coordinates of solid hydrogen in phase III with $P6_122$ space group at 200 GPa.

Atom	Position	x/a	y/b	z/c	Atom	Position	x/a	y/b	z/c
H1	1a	0.3313	0.0593	0.6582	H2	1a	0.8146	0.3381	0.6696
H3	1a	0.9407	0.2720	0.9915	H4	1a	0.6619	0.4765	0.0029
H5	1a	0.7280	0.6687	0.3249	H6	1a	0.5235	0.1854	0.3363
H7	1a	0.6687	0.9407	0.1582	H8	1a	0.1854	0.6619	0.1696
H9	1a	0.0593	0.7280	0.4915	H10	1a	0.3381	0.5235	0.5029
H11	1a	0.2720	0.3313	0.8249	H12	1a	0.4765	0.8146	0.8363
H13	1a	0.0593	0.3313	0.6751	H14	1a	0.3381	0.8146	0.6637
H15	1a	0.2720	0.9407	0.3418	H16	1a	0.4765	0.6619	0.3304
H17	1a	0.6687	0.7280	0.0085	H18	1a	0.1854	0.5235	0.9971
H19	1a	0.9407	0.6687	0.1751	H20	1a	0.6619	0.1854	0.1637
H21	1a	0.7280	0.0593	0.8418	H22	1a	0.5235	0.3381	0.8304
H23	1a	0.3313	0.2720	0.5085	H24	1a	0.8146	0.4765	0.4971
H25	1a	0.8482	-0.0000	0.5000	H26	1a	0.6011	-0.0000	0.5000
H27	1a	0.0000	0.8482	0.8333	H28	1a	-0.0000	0.6011	0.8333
H29	1a	0.1518	0.1518	0.1667	H30	1a	0.3989	0.3989	0.1667
H31	1a	0.1518	-0.0000	-0.0000	H32	1a	0.3989	-0.0000	-0.0000
H33	1a	0.0000	0.1518	0.3333	H34	1a	0.0000	0.3989	0.3333
H35	1a	0.8482	0.8482	0.6667	H36	1a	0.6011	0.6011	0.6667

of $C2/c$-24, the currently favored candidate for phase III known at present, are also presented in Table 1. The results show excellent consistency with previous observations of phase III with $P6_122$ space group [33]. The primitive cells of phase III with $P6_122$ space group and $C2/c$-24 share a high degree of similarity, with minor variations observed in the c axis length (50% longer in phase III with $P6_122$ structure due to two additional layers) and monoclinic distortion in $C2/c$-24. The volume per proton in phase III with $P6_122$ structure is only slightly larger (about 0.13%) than that in $C2/c$-24. Additionally, the bond lengths (BL) between hydrogen of phase III with $P6_122$ space group are only 0.83% larger than that of $C2/c$-24. All these indicate that phase III with $P6_122$ space group is a highly competitive candidate structure for phase III [9,33].

To investigate the structural stability of phase III with $P6_122$ space group structure, a series of total energy calculations were performed at various pressures around the experimental data. The enthalpy energy per proton was then determined using the following expression;

$$E_{ent} = \frac{E_{total} - nE_{\mathrm{H}}}{n}, \tag{1}$$

where E_{total} and E_{H} denote the total energies of solid hydrogen in phase III with $P6_122$ space group and a single H atom, respectively. n represents the number of H atoms. The calculated enthalpy energy per proton is depicted in Fig. 2(a). One can clearly see that E_{ent} increases smoothly with increasing pressure. Under 200 GPa, the enthalpy energy is negative, indicating an exothermic formation process for phase III with $P6_122$ space group, in good agreement with previous research that reported the thermodynamic stability of the phase III with $P6_122$ space group at pressures below 200 GPa at T = 0 K [33]. Conversely, positive

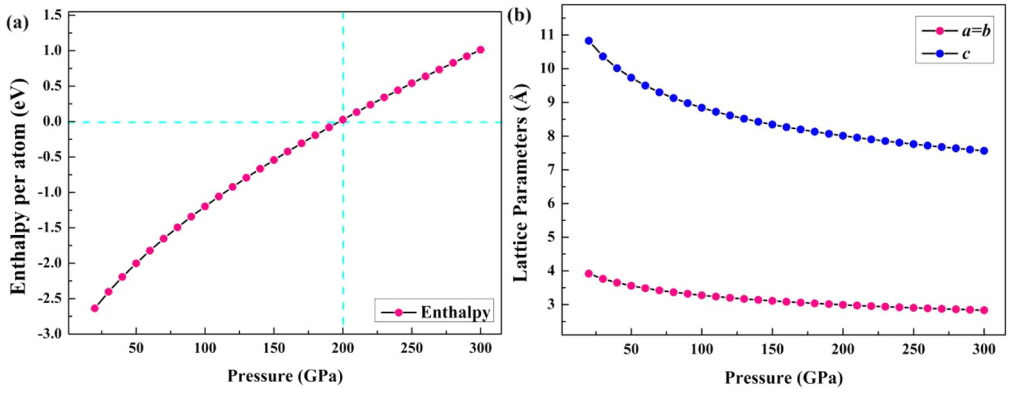

Fig. 2. The calculated (a) enthalpy and (b) lattice parameter of layered hydrogen in phase III with $P6_122$ space group as a function of pressure.

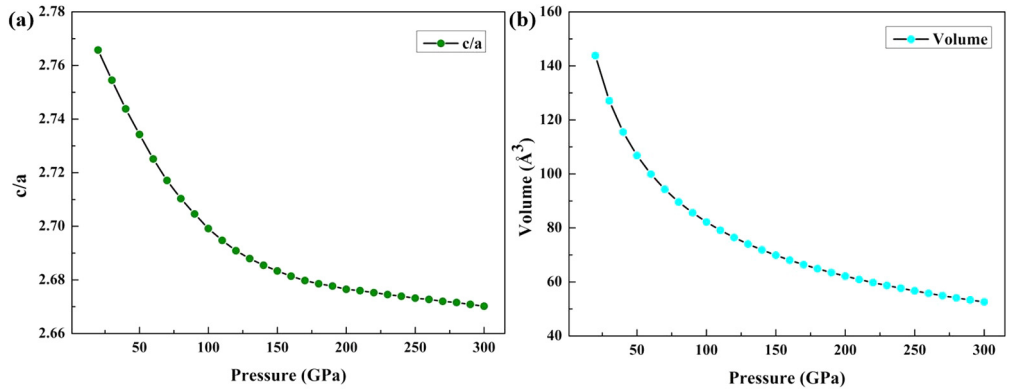

Fig. 3. The calculated (a) *c/a* and (b) pressure vs volume curves of layered hydrogen in phase III with $P6_122$ space group as a function of pressure.

values above 200 GPa imply that the formation of phase III with $P6_122$ structure is an endothermic process.

Fig. 2(b) shows the optimized lattice parameters (*a*, *b* and *c*) as a function of pressure. The lattice parameters decrease with increasing pressure, with a slightly higher decrement observed for *c*. This implies the presence of anisotropic property in phase III with $P6_122$ space group. Fig. 3(a) displays the *c/a* ratio of the hexagonal cell, which demonstrates a monotonic decrease below 100 GPa and a slower decrease beyond 100 GPa, suggesting that phase III with $P6_122$ crystal becomes increasingly anisotropic with pressure. Additionally, the obtained *c/a* ratio for phase III with $P6_122$ space group is significantly larger than the value of 1.633 of ideal hcp structure. Fig. 3(b) illustrates the pressure-volume relation (*P-V*) for solid hydrogen in phase III with $P6_122$ space group, which reveals that solid hydrogen for phase III with $P6_122$ space group is more compressible below 100 GPa compared to the range of 100∼300 GPa. We believe the pressure-volume equation of state in the range of 50 GPa ∼ 300 GPa can well describe the compression of molecular hydrogen in phase III with $P6_122$ space group at high pressure, since the compression mainly occurs between 50 GPa and 350 GPa.

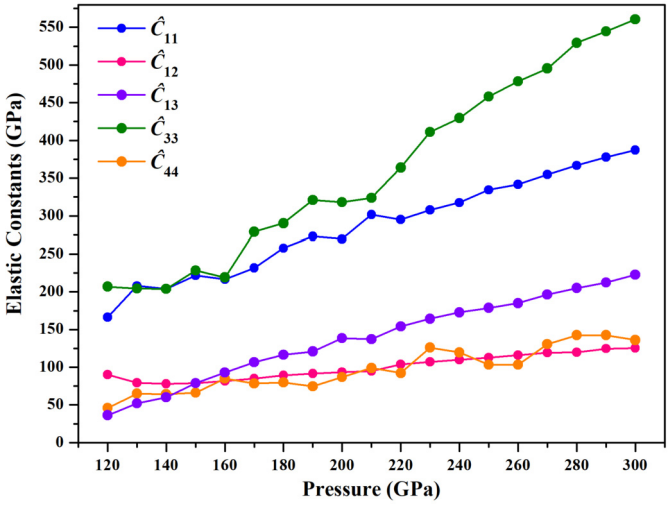

Fig. 4. Calculated elastic constants of layered hydrogen in phase III with $P6_122$ space group as a function of pressure.

3.2. Elastic behavior of solid hydrogen in phase III with $P6_122$ space group at high pressure

Elastic constants are not only important for understanding the bonding feature and anisotropy between adjacent atomic planes, but they also provide insight into the resistance and mechanical characteristics of materials under external stress or pressure, which further describes the stability of the material against elastic deformation [39,40]. It is worth pointing out that in the present work the elastic constants under hydrostatic pressure *P* at zero temperature are unified and simplified by the use of the Gibbs free energy *G* [41]. That is to say the equilibrium structure at each pressure *P* is not at a minimum of *E* for the solid hydrogen in phase III with $P6_122$ space group, but it is the values of the lattice constants *a* and *c* at which $G(a, c; P) \equiv E(a, c) + PV(a, c)$ has a minimum. Besides, the elastic constants are not evaluated as usual by second derivatives of *E* with respect to strains [40,42]. Rather they are given by second derivatives of the minimum of G at *P*. We define $\hat{C}_{ij} \equiv (1/V)\partial^2 G(a, c; P)/(\partial\varepsilon_i\partial\varepsilon_j)$ and $C_{ij} \equiv (1/V)\partial^2 E(a, c)/(\partial\varepsilon_i\partial\varepsilon_j)$, then the modified elastic constants $\hat{C}_{ij}$ equal to $C_{ij}+(P/V)\partial^2 V(a, c)/\partial\varepsilon_i\partial\varepsilon_j$ [41].

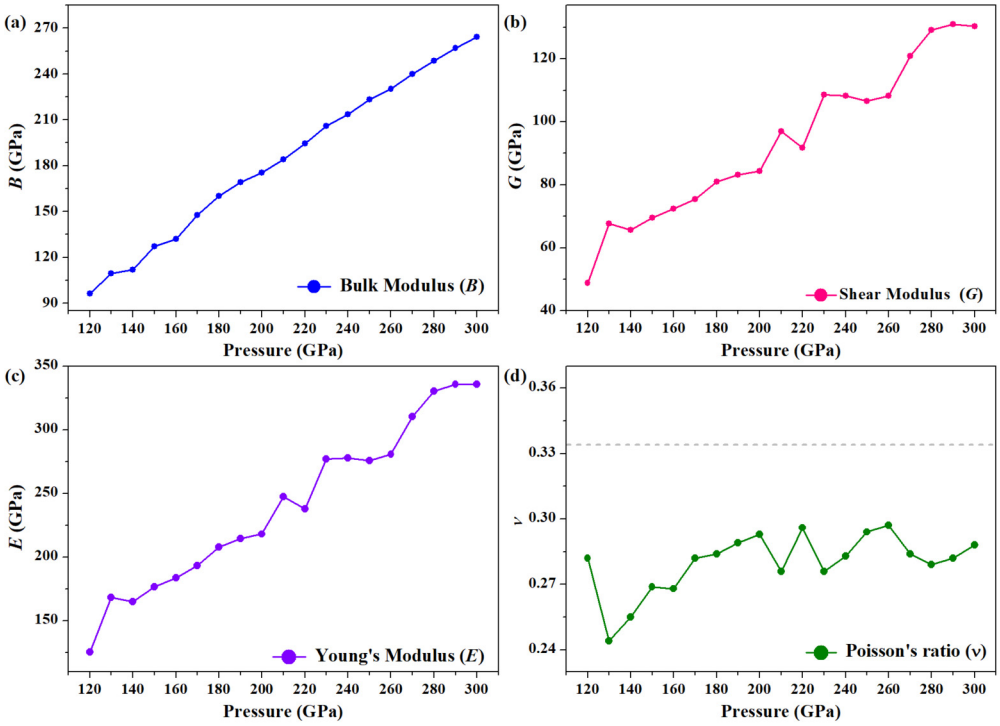

Fig. 5. The calculated (a) bulk moduli B, (b) shear moduli G, and (c) Young's modulus E of layered hydrogen molecular in phase III with $P6_122$ space group as a function of pressure, respectively.

In the case of solid hydrogen in phase III with $P6_122$ space group, five independent elastic constants, $\hat{C}_{11}$, $\hat{C}_{12}$, $\hat{C}_{13}$, $\hat{C}_{33}$, and $\hat{C}_{44}$, can determined by selectively imposing strains either individually or in combination along specific crystallographic directions. Table SI in supporting information illustrates the deformations employed in determining $2\times(\hat{C}_{11}+\hat{C}_{12})$, $2\times(\hat{C}_{11}-\hat{C}_{12})$, $\hat{C}_{33}$, $4\times\hat{C}_{44}$ and $(\hat{C}_{11}+2\hat{C}_{13}+\hat{C}_{33})$, which leads to the determination of all the elastic stiffness constants. These elastic constants can be calculated for solid hydrogen in phase III with $P6_122$ space group by selecting a proper set of strains $\{e_i, i=1,\cdots,6\}$ from the following five different strains (refer to Table SI),

$$\begin{aligned}&\sigma^1=(\delta,\delta,0,0,0,0), \quad \sigma^2=(\delta,-\delta,0,0,0,0),\\ &\sigma^3=(0,0,\delta,0,0,0), \quad \sigma^4=(0,0,0,\delta,0,0),\\ &\sigma^5=(\delta,\delta,\delta,0,0,0),\end{aligned} \tag{2}$$

where the Voigt notation has been used. In order to avoid the influence of high order terms on the estimated elastic constants, the small strains within $\pm1.5\%$ are used. Hence the strain amplitude δ is varied in step of 0.006 from -0.036 to 0.036 and the total energies $G(V_0,\sigma)$ at these strain steps are calculated and fitted through the strains with the corresponding parabolic equations of $\Delta G/V_0$ using equations in Table SI to yield the required second-order elastic constants. In order to ensure accurate results, relaxations of the coordinated H atoms in the strained lattice are carried out during the calculations for all elastic constants of solid hydrogen in phase III with $P6_122$ space group.

Fig. 4 illustrates the pressure dependence of the calculated elastic constants for solid hydrogen in phase III with $P6_122$ space group. As shown in the plot, all these five elastic constants exhibit a monotonic increase with increasing pressure. Specifically, $\hat{C}_{33}$ exhibits the biggest increase rate which is approximately 2.183, followed by $\hat{C}_{13}$ with the slop of 1.158, while $\hat{C}_{12}$, $\hat{C}_{13}$ and $\hat{C}_{44}$ exhibit relatively smaller increase rates of ∼0.281, ∼1.00, and ∼0.488, respectively. The smaller increasing rate for the value of $\hat{C}_{44}$ implies the shear deformation increase faster with the increase of pressure, leading the instability of the structure with external pressure. The usual Born conditions of mechanical stability remain valid for any pressure when applied to the elastic constants from G [41,43–45]:

$$\begin{aligned}&\hat{C}_{11}>0, \quad \hat{C}_{33}>0, \quad \hat{C}_{44}>0, \quad \hat{C}_{11}>|\hat{C}_{12}|, \quad \text{and}\\ &(\hat{C}_{11}+2\hat{C}_{12})\times\hat{C}_{33}>2\hat{C}_{13}^2.\end{aligned} \tag{3}$$

One can see solid hydrogen in phase III with $P6_122$ space group is stable within the pressure range of 120−300 GPa, based on the elastic constants calculated. Our results indicate that $\hat{C}_{11}$ is extraordinarily larger than $\hat{C}_{12}$ throughout the pressure range studied, revealing that the bonding strengths along the [100], [010] and [001] crystallographic directions are considerably stronger than those along the [011], [101] and [110] directions [39]. $\hat{C}_{44}>0$ is fulfilled, implying the shear strain in [100] plane does not cause mechanical instability under the corresponding pressure range. The shear elastic constant in [001] plane is obtained via $\hat{C}_{66}$ = $1/2(\hat{C}_{11}$-$\hat{C}_{12})$. The positive values of $\hat{C}_{66}$ illustrate that the shear strain in [001] plane does not cause mechanical instability when the pressure is below 300 GPa. While the enthalpy differences for solid hydrogen in phase III with $P6_122$ space group are positive in the pressure range of 200∼300 GPa, which implies that the structure of $P6_122$ space group of hydrogen can be a metastable structure in the pressure range between 200 to 300 GPa. It is also confirmed by the softening of phonon dispersion branches in Fig. 10.

Following the determination of elastic constants at varying pressures, we proceed to calculate the polycrystalline bulk modulus (B), shear modulus (G) as function of pressure, which can describe the response to compress and shear stress of solid hydrogen in phase III with $P6_122$ space group. These calculations are performed using the Voigt-Geuss-Hill (VRH) approximations as shown in the following equations [46],

$$B_V=(1/9)[2(\hat{C}_{11}+\hat{C}_{12})+4\hat{C}_{13}+\hat{C}_{33}], \tag{4}$$

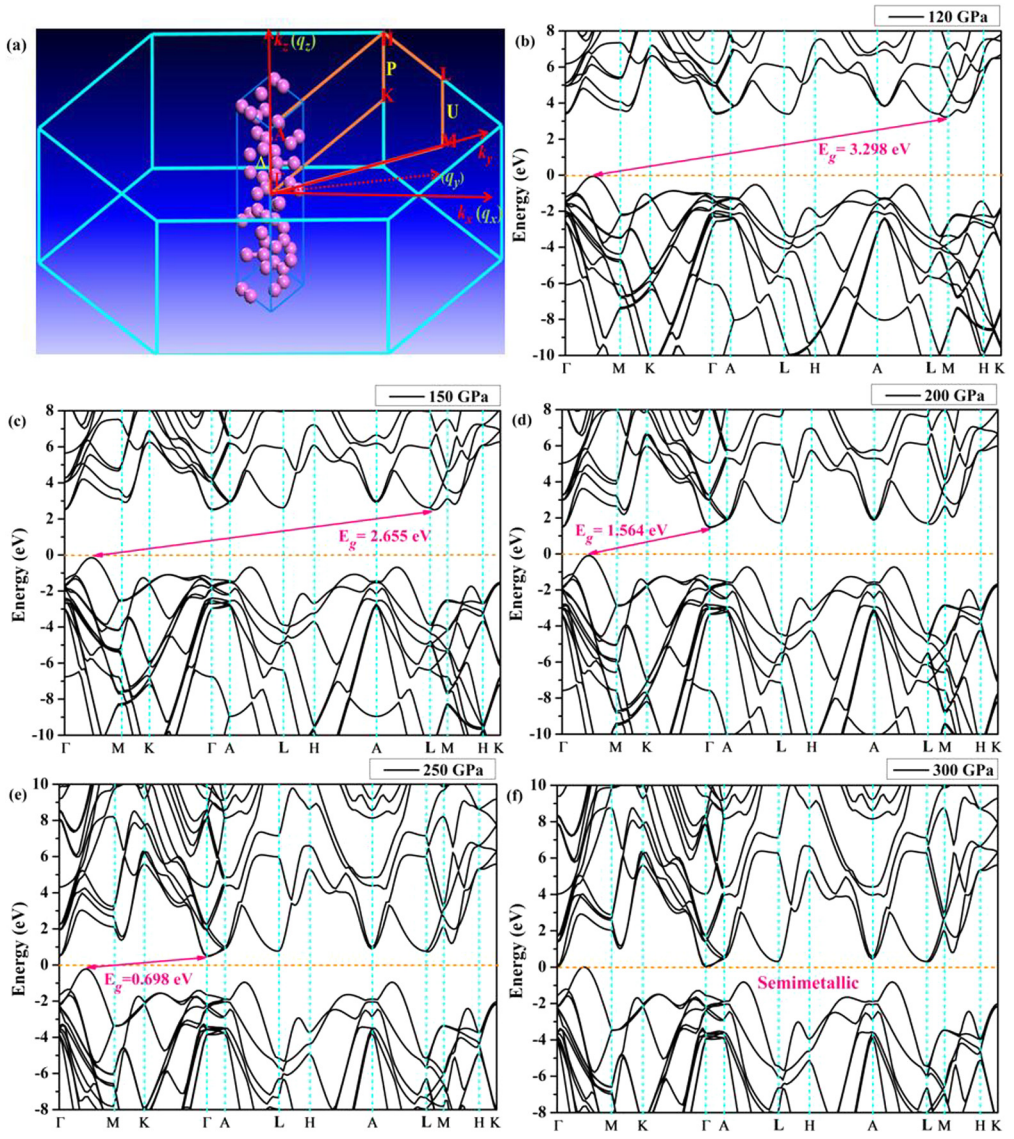

Fig. 6. (a) Three-dimensional bulk Brillouin zone (BZ) in which high-symmetry points are indicated. The orange lines indicate the high-symmetry lines of the BZ. q_x, q_y, and q_z are the basis vectors for an inverted space. k_y is perpendicular to k_x and k_z. Here, the cross points of orange and cyan lines denote paired Weyl points, which are symmetric about the k_z = 0 plane. Band structures of solid hydrogen in phase III with $P6_122$ space group under (b) 120 GPa, (c) 150 GPa, (d) 200 GPa, (e) 250 GPa and (f) 300 GPa, respectively.

$$B_R = C^2/M, \tag{5}$$

$$G_V = (1/30)(M + 12\hat{C}_{44} + 12\hat{C}_{66}), \tag{6}$$

$$G_R = (5/2)[C^2\hat{C}_{44}\hat{C}_{66}]/[3B_V\hat{C}_{44}\hat{C}_{66} + C^2(\hat{C}_{44} + \hat{C}_{66})], \tag{7}$$

$$C^2 = (\hat{C}_{11} + \hat{C}_{12})\hat{C}_{33} - 2\hat{C}_{13}^2, \tag{8}$$

$$M = \hat{C}_{11} + \hat{C}_{12} + 2\hat{C}_{33} - 4\hat{C}_{13}. \tag{9}$$

The bulk modulus (B) and shear modulus (G) are then obtained by

$$B = 1/2(B_V + B_R), \quad G = 1/2(G_V + G_R). \tag{10}$$

Correspondingly, Young's modulus (E), which measures the response to linear stress, and Poisson's ratio (ν) which describes the phenomenon of deformation perpendicular to the loading direction when the material is compressed or stretched can be calculated by the following definition:

$$E = \frac{9BG}{3B + G}, \tag{11}$$

$$\nu = \frac{3B - 2G}{2(3B + G)}. \tag{12}$$

The calculated results are depicted in Fig. 5. Distinctly, the deduced bulk moduli B increases linearly with pressure, while shear moduli E increases monotonically with slightly discontinuity, as shown in Fig. 5(a) and 5(c), respectively. The increasing rate of B is approximately two times larger than that of shear moduli E. Pugh criteria is widely used to identify the intrinsic ductile to brittle transition as a function of elastic properties, since the values of B and G represent the ability to resist external pressures and shearing forces, respectively [47]. The critical value of the ratio B/G is about 1.75, indicating that materials with B/G > 1.75 are ductile whereas those with B/G < 1.75 are brittle [47,48]. Our calculated average value of B/G almost reaches 2 (∼1.947) in the pressure range of 120 GPa to 300 GPa, which implies phase III with $P6_122$ structure is a ductile material. Additionally, the predicted values of Young's modulus E increase sharply from ∼125 GPa to ∼335 GPa with increasing pressure, indicating the ability to resist deformation is strongly enhanced with pressure. Regarding to the

Poisson's ratio ν, it is well known that the material which has much smaller shear moduli compared with the bulk moduli, its Poisson's ratios ν is usually close to 1/3. For the present solid hydrogen system, the calculated shear modulus G is much lower than the bulk modulus B. Thus, the predicted average value of 0.28 with increasing pressure for the Poisson's ration ν in Fig. 5(d) can be well understandable and reasonable. Furthermore, the microcracks in materials could be induced by the elastic anisotropy, thus the anisotropic factors of solid hydrogen in phase III with $P6_122$ space group as the function of pressure are calculated according to the following equation to understand its mechanical durability,

$$A = \frac{2\hat{C}_{44}}{\hat{C}_{11} - \hat{C}_{12}}, \tag{13}$$

here, the factor A with 1.0 indicates elastic isotropic for crystal while a value different from 1.0 is for elastic anisotropy. The calculated results are presented in Fig. S1. One can see from Fig. S1 that the calculated values of A largely fluctuate around 1, indicating solid hydrogen in phase III with $P6_122$ space group is elastically anisotropic, which is consistent with the above conclusion for the changes of lattice parameters as the function of pressure. The further comparison with experimental results for the mechanical properties of solid hydrogen in phase III with $P6_122$ space group is necessary. We expect the present elastic constants and elastic moduli can provide a reference for future experimental measurements.

3.3. Electronic structure of solid hydrogen in phase III with $P6_122$ space group at high pressure

All the macroscopical properties of materials, such as elasticity, hardness, as well as conductivity originate from their electronic structure properties and the feature of the chemical bonding. Hence it is necessary to investigate the electronic structure of solid hydrogen in phase III with $P6_122$ space group. The three dimensional bulk Brillouin zone (BZ) of solid hydrogen in phase III with $P6_122$ space group and the corresponding band structures in the high-symmetry directions in the BZ are displayed in Fig. 6. The energy scale is in eV, and the valence band maximum is set to be the Fermi energy (E_f), indicating the bands below E_f are all occupied. It can be clearly seen the band features are very similar with an indirect bandgaps in the pressure range of 120∼290 GPa. The calculated bandgap at 120 GPa is 3.398 eV, which shows a topological insulating property. While it decreases to 0.122 eV at 290 GPa as a topological semiconductor. Moreover, the bandgaps of solid hydrogen in phase III with $P6_122$ space group exhibit a linear decrease from 120 GPa to 290 GPa, as shown in Fig. 7. Most importantly, upon compression up to 300 GPa, the bandgap disappeared owing to the valance band and the conduction band overlapping in different momentum point. Thus, the band structure displays a semimetallic behavior, as shown in Fig. 6(f). The cause of this metallicity is partly attributed to the aligned inter- and intralayer molecules along the c axis, as shown in Fig. 1. Consequently, there is a difference in the electron density polarization due to the intermolecular interactions between the insulating and semimetallic structures (which will be discussed latter in Fig. 9). The bandgap revolutions of solid hydrogen in phase III with $P6_122$ space group from insulating phase under low pressures to monoatomic metallic phase at 290 GPa are detailly presented in Fig. 7.

Importantly, the nontrivial topology is observed in solid hydrogen in phase III with $P6_122$ space group, which is exhibited by a large number of Weyl point nodes along the $\Gamma - \Delta -$ A and M $-$ U $-$ L lines in the conduction bands in the pressure domain of 120∼290 GPa. The accordion dispersion is clearly visible about E_f,

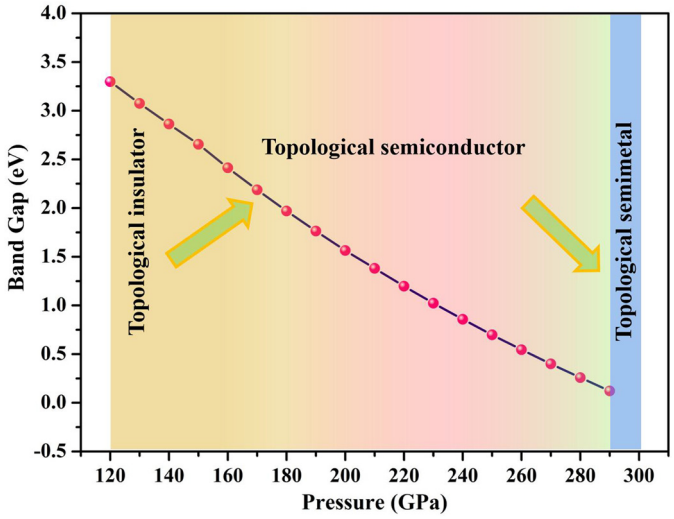

Fig. 7. The calculated bandgap of solid hydrogen in phase III with $P6_122$ space group as a function of pressure.

which is presented in Fig. 8 with more details. While it is less clear below E_f, where the bands are not well separated in energy (not shown in the present work). As shown in Fig. 8(a-e), one can observe a group of five connected bands along the $\Gamma - \Delta -$ A line, which is invariant under the screw rotation $C_{6,1}$. While, along the M $-$ U $-$ L line which is symmetric under the screw rotation $C_{6,1}^3$, there are groups of four bands sticking together with an hourglass dispersion, forming four crossings. Nevertheless, all bands, forming Weyl point nodes along the $\Gamma - \Delta -$ A and M $-$ U $-$ L lines, are required by symmetry. This behavior has been referred as twisted equivariant K-theory [49]. By the bulk-boundary correspondence these Weyl point nodes give rise to arc surface states.

To a great extent, the electronic distribution and the interaction between H atoms are the main contributors in the enthalpy energy. Thus we first plot the valence charge density in (001) plane of solid hydrogen in phase III with $P6_122$ space group, as shown in Fig. 9. Obviously, all these five contours plots of charge density distributions show that there is a remarkable s orbital electronic bridge between H1 and H2 atoms, which represents the covalent bonding nature between H1 and H2 and further forms a pseudo "H_2" molecule with bond length less than 0.74 Å. Besides, there is a elliptical distribution around the "H_2" molecule with slight deformation towards the directions of their nearest neighboring H_2 molecules. In the insulating phases, the charge density around the "H_2" molecules is higher within each layer with increasing pressure, while there are hardly a valence charge in the trigonal interstitial region, such as charge density distribution at 120 GPa in Fig. 9(a) with the three arrows. On the other hand, in the semimetallic phase at 300 GPa, the charge density is partly channeled into the interlayer space since there are some valence charge in the interstitial region, as shown in Fig. 9(e) with the three arrows. The Bader topological charge analysis could decompose the charge density into atomic components based on topological features of the charge density [50,51]. Thus we systematically study the atomic charges for H atoms under different pressures. It is found there are respectively 0.743 and 1.222 electrons around the H1 and H2 atoms at 120 GPa, which indicates that approximately 0.222 electrons are transferred from H1 to its nearest H2 atom. While there are only 0.080 electrons transferred from H1 to H2 by applying the 300 GPa compression. As a consequence, the ionicity of H1-H2 bond is gradually decreased while the covalent character is strengthened with increasing the pressure from 120 GPa to 300 GPa. Additionally, the bonding length of H1-H2 is grad-

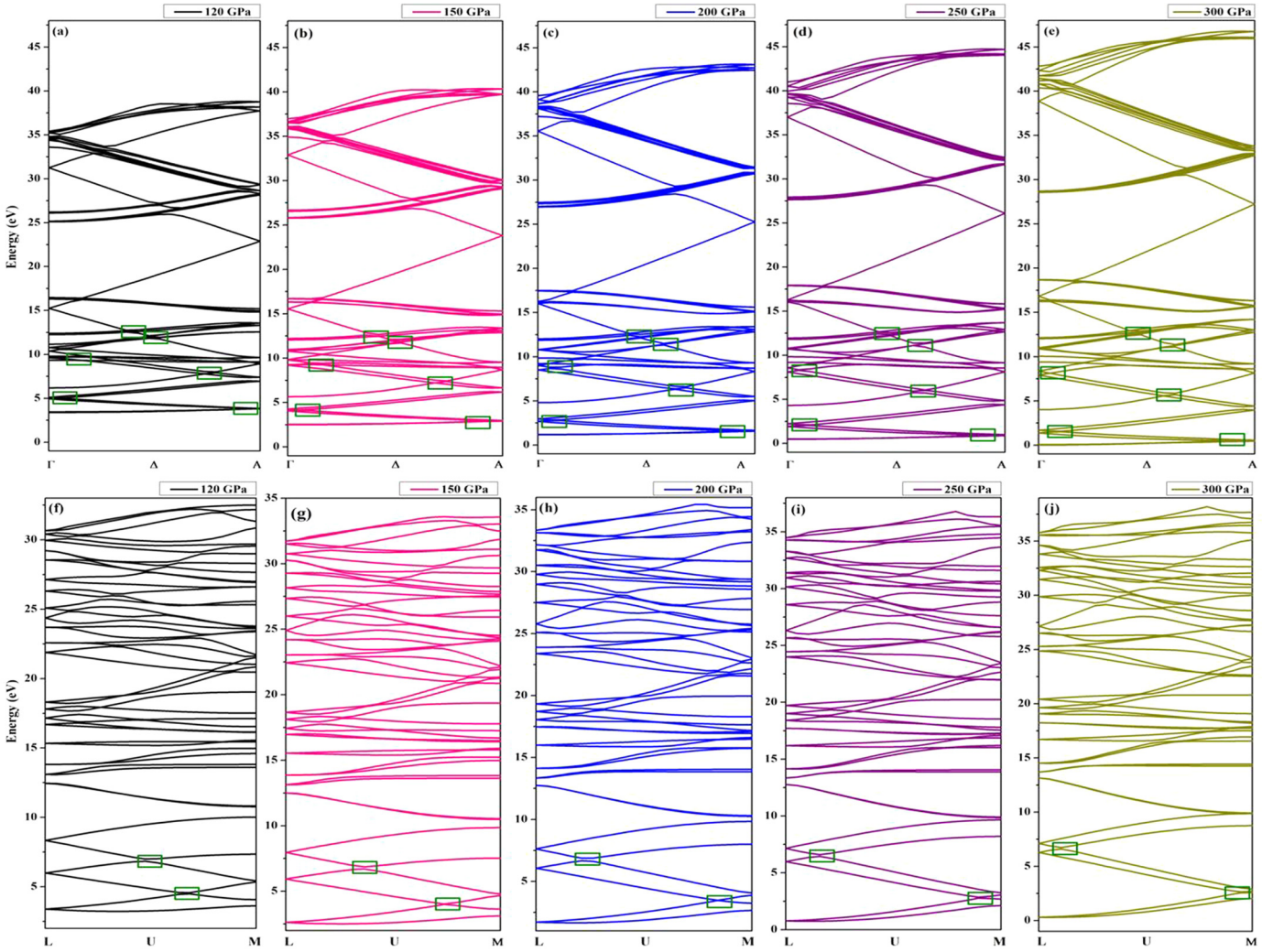

Fig. 8. Electronic band structures of solid hydrogen in phase III with $P6_122$ space group under 120, 150, 200, 250, and 300 GPa, respectively. The band crossings along the $\Gamma-\Delta-$ A lines (top panel) are symmetry-enforced by the screw rotations $C_{6,1}$. The band crossings along the M−U−L lines (bottom panel) are symmetry-enforced by the screw rotations $C^3_{6,1}$. The green open symbols represent the Weyl points formed by the second and third, fourth, and fifth lowest bands, respectively, which are part of Weyl nodal lines.

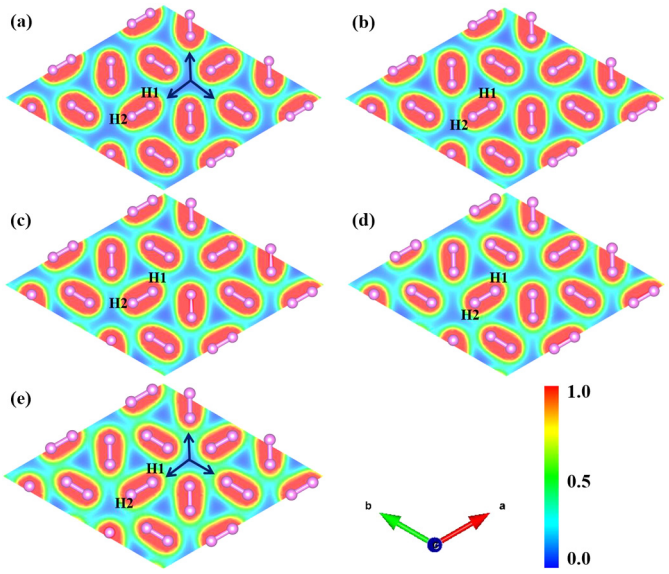

Fig. 9. Contour plots of charge density distributions of solid hydrogen in phase III with $P6_122$ space group inside the (001) plane under (a) 120 GPa, (b) 150 GPa, (c) 200 GPa, (d) 250 GPa and (e) 300 GPa, respectively.

ually increased from 0.708 Å under 120 GPa to 0.735 Å under 300 GPa.

3.4. Phonon dispersion curves and thermodynamic stability

To the best our knowledge, phonon spectra shows a significant relation with dynamic stability, phase transition, thermoelectric effect and superconductivity [52,53]. Thus, in the present work the phonon dispersion curves for solid hydrogen in phase III with $P6_122$ space group are further investigated using the density functional perturbation theory (DFPT) with the help of PHONOPY package [54]. To reach high accuracy, a 2×2×1 extension of conventional unit cell (including 144 atoms) and 5×5×5 Monkhorst-Pack *k*-point mesh for the BZ integration are adopted to calculate the force constants. The calculated phonon curves along Γ−M−K−Γ−A−L−H−A−L−M−H−K directions under 100 GPa, 120 GPa, 150 GPa, 200 GPa, 250 GPa and 300 GPa are displayed in Fig. 10. Overall speaking, the behaviors of the phonon as a function of pressure are similar with an evident gap between the optic modes and the acoustic branches. The obtained phonon dispersion shows that solid hydrogen in phase III with $P6_122$ structure is dynamically unstable at selected pressure of 100 GPa, as shown in Fig. 10(a). The transverse acoustic (TA) mode close to Γ point becomes imaginary along the Γ− M, Γ− K and Γ− A directions.

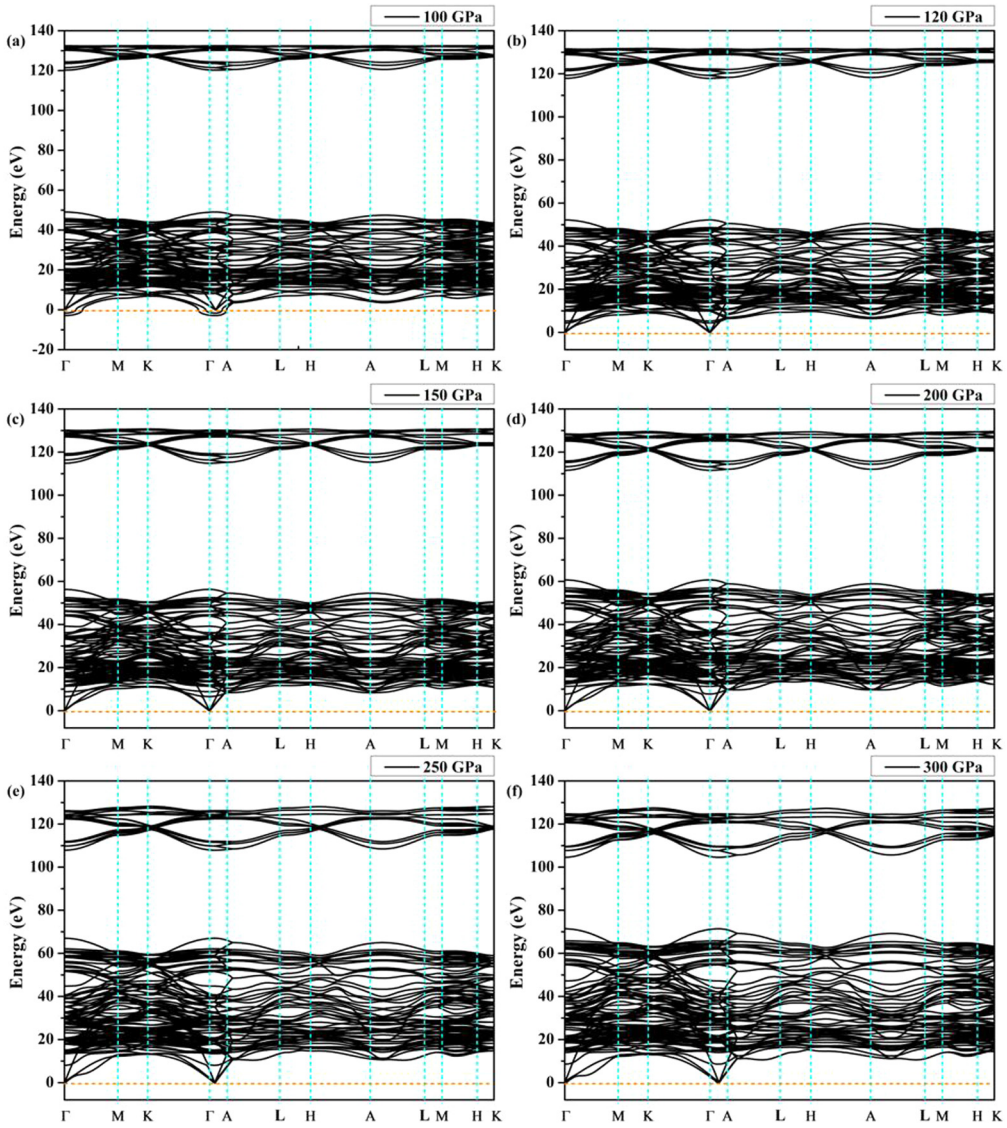

Fig. 10. The calculated phonon dispersion curves of solid hydrogen in phase III with $P6_122$ space group at (a) 100 GPa, (b) 120 GPa, (c) 150 GPa, (d) 200 GPa, (e) 250 GPa and (f) 300 GPa, respectively.

The minimum of the TA branch locates at the Γ− A direction. While, no imaginary frequencies are observed in the pressure domain of 120∼300 GPa at 0 K, as clearly indicated in Fig. 10(b-f). Besides, after applying pressure, the acoustic and optic branches of phonon undergo that frequencies slightly shift upward and downward, respectively, indicating the enhancing of atomic interactions. Two lowest acoustic branches exhibit soft oscillating mode along the Γ−M and Γ−A directions with increasing the pressure. This information is critical important to analyze the phase transformation. In order to further figure out the effects of low pressure on dynamical stability of solid hydrogen in phase III with $P6_122$ space group, the calculated phonon dispersion curves at 50 GPa and 80 GPa pressure domains are displayed in Fig. S2. One can notice that the TA mode close to Γ point also becomes imaginary at 80 GPa along the Γ−M, Γ−K, Γ−A, Γ−H, and Γ−L directions. Additionally, this similarity of the softening in TA branches is clearly observed at 50 GPa in Fig. S2(a). Thus, phonon spectrum results illustrate that phase III with $P6_122$ structure for solid hydrogen is dynamically unstable till being compressed over 120 GPa, which is well consistent with the above results about the mechanical stability analysis for solid hydrogen in phase III with $P6_122$ space group and the result of enthalpy difference of various phases of hydrogen in Ref. [9,33].

4. Conclusion

To conclude, this study employs first-principles calculations to comprehensively analyze high-pressure hydrogen with hexagonal symmetry, specifically phase III with $P6_122$ space group, as a candidate structure for phase III. We systematically investigate the structure, energetic, mechanical, electronic and thermodynamic properties of solid hydrogen in phase III with $P6_122$ space group as a function of pressure. Our results indicate that phase III with $P6_122$ space group is both mechanically and thermodynamically stable in the pressure range of 120 ∼ 300 GPa, with a clear volume contraction as pressure increases. Furthermore, we find the bulk modulus B, shear modulus G and Young's modulus E increase linearly as pressure increases. The calculated band structures demonstrate a strong reduction in the bandgap for phase III with $P6_122$ structure as pressure increases, indicating a phase transition from a topological insulator to a topological semiconductor. As pressures exceeding 300 GPa, phase III with $P6_122$ structure becomes

a topological semimetal with bands crossing the Fermi energy. Accordingly, the electron density accumulates between the "H_2" molecules within each layer in the insulating phase, whereas the density is channeled into the interlayer space in the semimetallic phase. Our phonon spectrum results confirm that phase III with $P6_122$ space group is dynamically stable in the pressure domain of 120∼300 GPa, which is in agreement with our mechanical stability analysis. Moreover, since this system size with 36 atoms per primitive cell has been barely explored previously in hydrogen research, our study provides valuable insights to interpret experimental data.

CRediT authorship contribution statement

Xiao-Yong Yang: Writing – original draft, Formal analysis, Data curation. **Rajeev Ahuja:** Writing – review & editing, Supervision, Software, Resources, Project administration, Methodology, Funding acquisition, Conceptualization. **Wei Luo:** Writing – review & editing, Supervision, Software, Resources, Project administration, Investigation, Funding acquisition, Data curation, Conceptualization.

Declaration of competing interest

The authors declare that they have no known competing financial interests or personal relationships that could have appeared to influence the work reported in this paper.

Data availability

Data will be made available on request.

Acknowledgements

W.L. and R.A. acknowledge the support from the Swedish Research Council (Grant Nos. VR-2021-00665, VR-2020-04410, and VR-2016-06014) for financial support and J. Gust. Richert Stiftelse, Sweden (2021-00665). X.Y. thanks funding from the National Natural Science Foundation of China (Grant No. 11705152). The computations resources are provided by the Swedish National Infrastructure for SNIC, HPC2N, and UPPMAX.

Appendix A. Supplementary material

Supplementary material related to this article can be found online at https://doi.org/10.1016/j.physleta.2023.129040.

References

[1] R.J. Hemley, H.K. Mao, Phase transition in solid molecular hydrogen at ultrahigh pressures, Phys. Rev. Lett. 61 (1988) 857.
[2] R.J. Hemley, H.K. Mao, J.F. Shu, Low-frequency vibrational dynamics and structure of hydrogen at megabar pressures, Phys. Rev. Lett. 65 (1990) 2670.
[3] H.K. Mao, R.J. Hemley, Ultrahigh-pressure transitions in solid hydrogen, Rev. Mod. Phys. 66 (1994) 671.
[4] P. Loubeyre, R. LeToullec, D. Hausermann, M. Hanfland, R.J. Hemley, H.K. Mao, L.W. Finger, X-ray diffraction and equation of state of hydrogen at megabar pressures, Nature 383 (1996) 702–704.
[5] H.E. Lorenzana, I.F. Silvera, K.A. Goettel, Orientational phase transitions in hydrogen at megabar pressures, Phys. Rev. Lett. 64 (1990) 1939.
[6] A.F. Goncharov, R.J. Hemley, H.K. Mao, J. Shu, New high-pressure excitations in parahydrogen, Phys. Rev. Lett. 80 (1998) 101.
[7] X.D. Liu, R.T. Howie, H.C. Zhang, X.J. Chen, E. Gregoryanz, High-pressure behavior of hydrogen and deuterium at low temperatures, Phys. Rev. Lett. 119 (2017) 06530.
[8] R.T. Howie, C.L. Guillaume, T. Scheler, A.F. Goncharov, E. Gregoryanz, Mixed molecular and atomic phase of dense hydrogen, Phys. Rev. Lett. 108 (2012) 125501.
[9] C. Ji, B. Li, W.J. Liu, J.S. Smith, A. Majumdar, W. Luo, R. Ahuja, J.F. Shu, J.Y. Wang, S. Sinogeikin, Y. Meng, V.B. Prakapenka, E. Greenberg, R.Q. Xu, X.R. Huang, W.G. Yang, G.Y. Shen, W.L. Mao, H.K. Mao, Ultrahigh-pressure isostructural electronic transitions in hydrogen, Nature 573 (2019) 558–562.
[10] C.J. Pickard, M. Martinez-Canales, R.J. Needs, Density functional theory study of phase IV of solid hydrogen, Phys. Rev. B 85 (2012) 214114.
[11] R.T. Howie, T. Scheler, C.L. Guillaume, E. Gregoryanz, Proton tunneling in phase IV of hydrogen and deuterium, Phys. Rev. B 8 (2012) 214104.
[12] P. Dalladay-Simpson, R.T. Howie, E. Gregoryanz, Evidence for a new phase of dense hydrogen above 325 gigapascals, Nature 529 (2016) 63–67.
[13] B. Monserrat, N.D. Drummond, P. Dalladay-Simpson, R.T. Howie, P.L. Róos, E. Gregoryanz, C.J. Pickard, R.J. Needs, Structure and metallicity of phase V of hydrogen, Phys. Rev. Lett. 120 (2018) 255701.
[14] M.I. Eremets, I.A. Troyan, Conductive dense hydrogen, Nat. Mater. 10 (2011) 927.
[15] M.I. Eremets, A.P. Drozdov, P.P. Kong, H. Wang, Semimetallic molecular hydrogen at pressure above 350 GPa, Nat. Phys. 15 (2019) 1246–1249.
[16] P. Loubeyre, F. Occelli, P. Dumas, Synchrotron infrared spectroscopic evidence of the probable transition to metal hydrogen, Nature 577 (2020) 631–635.
[17] R.P. Dias, I.F. Silvera, Observation of the Wigner-Huntington transition to metallic hydrogen, Science 355 (2017) 715–718.
[18] V. Natoli, R.M. Martin, D. Ceperley, Crystal structure of molecular hydrogen at high pressure, Phys. Rev. Lett. 74 (1995) 1601–1604.
[19] R.P. Dias, O. Noked, I.F. Silvera, Quantum phase transition in solid hydrogen at high pressure, Phys. Rev. B 100 (2019) 184112.
[20] K.A. Johnson, N.W. Ashcroft, Structure and bandgap closure in dense hydrogen, Nature 403 (2000) 632–635.
[21] S. Azadi, W.M.C. Foulkes, T.D. Kühne, Quantum Monte Carlo study of high pressure solid molecular hydrogen, New J. Phys. 15 (2013) 113005.
[22] R. Singh, S. Azadi, T.D. Kuhne, Anharmonicity and finite temperature effects on the structure, stability, and vibrational spectrum of phase III of solid molecular hydrogen, Phys. Rev. B 90 (2014) 014110.
[23] Y. Lu, F.W. Zheng, W. Yang, W. Kang, Z. Li, C. Wang, G.W. Gu, F.L. Tan, J.H. Zhao, C.L. Liu, C.W. Sun, P. Zhang, Temperature effect on the phase stability of hydrogen C_2/c phase from first-principles molecular dynamics calculations, J. Phys. Condens. Matter 32 (2020) 405404.
[24] H. Kitamura, S. Tsuneyuki, T. Ogitsu, T. Miyake, Quantum distribution of protons in solid molecular hydrogen at megabar pressures, Nature 404 (2000) 259.
[25] C.J. Pickar, R.J. Needs, Structure of phase III of solid hydrogen, Nat. Phys. 3 (2007) 473–476.
[26] K. Nagao, H. Nagara, Theoretical study of Raman and infrared active vibrational modes in highly compressed solid hydrogen, Phys. Rev. Lett. 80 (1998) 548–551.
[27] V. Gorelov, M. Holzmann, D.M. Ceperley, C. Pierleoni, Energy gap closure of crystalline molecular hydrogen with pressure, Phys. Rev. Lett. 124 (2020) 116401.
[28] I. Souza, R.M. Martin, Polarization and strong infrared activity in compressed solid hydrogen, Phys. Rev. Lett. 81 (1998) 4452.
[29] V. Natoli, R.M. Martin, D.M. Ceperley, Crystal structure of atomic hydrogen, Phys. Rev. Lett. 70 (1993) 1952.
[30] G.J. Ackland, J.S. Loveday, Structures of solid hydrogen at 300 K, Phys. Rev. B 101 (2020) 094104.
[31] H.X. Zong, H. Wiebe, G.J. Ackland, Understanding high pressure molecular hydrogen with a hierarchical machine-learned potential, Nat. Commun. 11 (2020) 5014.
[32] S. van de Bund, G.J. Ackland, Quadrupole arrangements and the ground state of solid hydrogen, Phys. Rev. B 101 (2020) 014103.
[33] B. Monserrat, R.J. Needs, E. Gregoryanz, C.J. Pickard, Hexagonal structure of phase III of solid hydrogen, Phys. Rev. B 94 (2016) 134101.
[34] B. Hammer, L.B. Hansen, J.K. Nørskov, Improved adsorption energetics within density functional theory using revised Perdew-Burke-Ernzerhof functionals, Phys. Rev. B 59 (1999) 7413.
[35] J.P. Perdew, K. Burke, M. Ernzerhof, Fluid vesicles in shear flow, Phys. Rev. Lett. 77 (1996) 3865–3868.
[36] J. Singh, S.S. Sahoo, K. Venkatakrishnan, G. Vaitheeswaran, D. Errandonea, High-pressure study of the aurophilic topological Dirac material AuI, J. Alloys Compd. 928 (2022) 167178.
[37] A. Togo, F. Oba, I. Tanaka, First-principles calculations of the ferroelastic transition between rutile-type and $CaCl_2$-type SO_2 at high pressures, Phys. Rev. B 78 (2008) 134106.
[38] C. Lee, W. Yang, R.G. Parr, Development of the Colle-Salvetti correlation-energy formula into a functional of the electron density, Phys. Rev. B 37 (1988) 785.
[39] B.T. Wang, R. Lizárraga, I.D. Marco, O. Eriksson, Phonon spectrum, thermodynamic properties, and pressure-temperature phase diagram of uranium dioxide, Phys. Rev. B 88 (2013) 104107.
[40] X.Y. Yang, Y. Lu, F.W. Zheng, P. Zhang, Mechanical, electronic, and thermodynamic properties of zirconium carbide from first-principles calculations, Chin. Phys. B 24 (2015) 116301.
[41] P.M. Marcus, Hong Ma, S.L. Qiu, On the importance of the free energy for elasticity under pressure, J. Phys. Condens. Matter 14 (2002) L525–L528.
[42] X.Y. Yang, Y. Liu, Q. Wei, T.R. Arslanov, J. Wärnå, Y. Yang, P. Zhang, Structural, electronic, mechanical and thermodynamic properties of U-Si intermetallic compounds: a comprehensive first principles calculations, Prog. Nucl. Energy 148 (2022) 104229.

[43] M. Boren, On the stability of crystal lattices. I., Math. Proc. Camb. Philos. Soc. 36 (1940) 160.
[44] G.V. Sin'ko, N.A. Smirnov, Relative stability and elastic properties of hcp, bcc, and fcc beryllium under pressure, Phys. Lett. Rev. 71 (2005) 214108.
[45] G.V. Sin'ko, N.A. Smirnov, Ab initio calculations of elastic constants and thermodynamic properties of bcc, fcc, and hcp Al crystals under pressure, J. Phys. Condens. Matter 14 (2002) 6989–7005.
[46] R. Hill, The elastic behaviour of a crystalline aggregate, Proc. Phys. Soc. A 65 (1952) 349–354.
[47] S.F. Pugh, Relations between the elastic moduli and the plastic properties of polycrystalline pure metals, Philos. Mag. 45 (1954) 823–843.
[48] X.Y. Yang, Y. Lu, F.W. Zheng, P. Zhang, First-principles study of the stability and diffusion properties of hydrogen in zirconium carbide, J. Nucl. Mater. 479 (2015) 130–136.
[49] J. Zhang, Y.H. Chan, C.K. Chiu, M.G. Vergniory, L.M. Schoop, A.P. Schnyder, Topological band crossings in hexagonal materials, Phys. Rev. Mater. 2 (2018) 074201.
[50] R.F.W. Bader, Atoms in Molecules: A Quantum Theory, Oxford University Press, New York, 1990, p. 155.
[51] X.Y. Yang, Y. Lu, P. Zhang, First-principles study of native point defects and diffusion behaviors of helium in zirconium carbide, J. Nucl. Mater. 485 (2015) 161–166.
[52] B.T. Wang, P. Zhang, Phonon spectrum and bonding properties of Bi_2Se_3: role of strong spin-orbit interaction, Appl. Phys. Lett. 100 (2012) 082109.
[53] X.Y. Yang, Y. Lu, M.L. Li, P. Zhang, First-principles study of migration and diffusion mechanisms of helium in α-Be, AIP Adv. 6 (2016) 035018.
[54] A. Togo, F. Oba, I. Tanaka, First-principles calculations of the ferroelastic transition between rutile-type and $CaCl_2$-type SiO_2 at high pressures, Phys. Rev. B 78 (2008) 134106.